THE ASTROPHYSICAL JOURNAL, 451:238–251, 1995 September 20

FOURIER TRANSFORM SPECTROSCOPY OF THE ORION MOLECULAR CLOUD CORE

E. SERABYN
Division of Physics, Mathematics, and Astronomy, California Institute of Technology, 320–47, Pasadena, CA 91125
AND
E. W. WEISSTEIN
Division of Geological and Planetary Sciences, California Institute of Technology, 170–25, Pasadena, CA 91125
Received 1994 December 12; accepted 1995 March 29

ABSTRACT

The near-millimeter and submillimeter wavelength emission-line spectrum of the Orion molecular cloud core has been measured at a resolution of 0.2 GHz with a new Fourier transform spectrometer at the Caltech Submillimeter Observatory. The broadband nature of the measured spectrum provides for a uniformly calibrated overview of the dominant broad-line radiators in the cloud core (excluding those molecules whose lines are obscured by our atmosphere). In total, 182 lines from 17 molecular species have been identified. Of these, CO accounts for the brightest lines, but the shock-enhanced SO_2 and SO molecules dominate the subterahertz line flux from the cloud core. In addition, highly excited lines of the "density tracers" CS and HCN are seen throughout the measured bands.

Subject headings: ISM: individual (Orion Nebula) — ISM: molecules — line: identification — radio lines: ISM

1. INTRODUCTION

Stars form in dense condensations (or "cores") within interstellar molecular clouds. The rich chemistry occurring in such cloud cores leads to the presence of numerous molecular species, which cool the gas by means of their line radiation (e.g., Blake et al. 1987, Fig. 1). The emerging radiation carries information on the clouds' physical and chemical state (Cernicharo 1991; Genzel 1991; Phillips & Keene 1992), but because of low gas temperatures ($\sim$50–200 K), thermal emission occurs at millimeter, submillimeter, and far-infrared wavelengths, a regime where technical obstacles, as well as poor atmospheric transmission, have impeded wideband spectral measurements.

Indeed, even though approximately 100 molecular species have now been identified in the interstellar medium (Irvine, Goldsmith, & Hjalmarson 1987; Turner & Ziurys 1988; van Dishoeck et al. 1993; Rohlfs & Wilson 1995) via targeted narrowband searches and time-intensive heterodyne surveys (Johansson et al. 1984; Sutton et al. 1985, 1991, 1995; Blake et al. 1986, 1987; Cummins, Linke, & Thaddeus 1986; Jewell et al. 1989; Turner 1989, 1991; Greaves & White 1991; Ziurys & McGonagle 1993; Groesbeck 1994; Schilke et al. 1995a), the total spectral coverage of extant millimeter/submillimeter observations nevertheless remains quite limited. This is due primarily to the narrow-band nature of the heterodyne receivers in standard use at these wavelengths. Wide-band spectra would be especially valuable in exploring the extensive submillimeter bands now accessible from high, dry observatory sites such as Mauna Kea, and so we have developed a moderate-resolution Fourier transform spectrometer (FTS) for near-millimeter and submillimeter wavelength astronomical observations. In the following, we briefly describe the FTS and present initial observations obtained therewith of the Orion molecular cloud core.

2. INSTRUMENTATION

Although millimeter and submillimeter wavelength observations of the interstellar medium (ISM) are now commonplace, nearly all such observations are made with a spectral resolving power, $R(=\nu/\Delta\nu$, with ν the frequency and $\Delta\nu$ the frequency resolution), that is either very high ($R > 10^5$ for heterodyne receivers) or very low ($R \leq 10$ for bandpass filter/bolometer systems). Intermediate-resolution observations are rare at these wavelengths (a notable exception being the *COBE* FIRAS spectrometer; Wright et al. 1991) but are common at infrared wavelengths, where the sizes of the necessary spectrometer components (which scale with λ for fixed R) become smaller and where heterodyne techniques become more difficult.

For wide-band studies of the ISM at near- and submillimeter wavelengths, an FTS (Schnopper & Thompson 1974; Brault 1985) offers several advantages in comparison with heterodyne receivers (Storey 1985). By far the most important advantage is the much larger bandwidth available with an FTS. In addition, problems associated with calibrating a double-sideband heterodyne response are completely absent, as there is no image band. Finally, with a broadband bolometric detector fed by a multimode horn antenna (Harper et al. 1976), the observing beamwidth becomes independent of frequency, ν, for $\nu \gg \nu_c$, where ν_c is the horn's cutoff frequency, thus providing a frequency-independent source coupling at high frequencies. All of these factors lead to a calibration which is uniform across a wide frequency range. FTS observations thus open up the possibility of measuring widely spaced rotational transitions of a given molecule with the same spectrometer and beam size, an arrangement that has obvious calibration advantages over multitransition data obtained with a series of different heterodyne receivers (which perhaps are also located at different telescopes), requiring a separate calibration of sideband ratio, beamwidth, and coupling efficiency for each line.

Of course, at long wavelengths, heterodyne receivers retain tremendous advantages in terms of resolving power and sensitivity. For a maximum scan length, L, of about 1 m, the resolving power of an FTS (given for one-sided scans by $R = 4L/1.2\lambda$; Schnopper & Thompson 1974; Brault 1985) is limited to $R \lesssim 10^4$ for subterahertz frequencies. While high by

infrared direct detection standards, this resolving power is well below typical heterodyne values, and so only moderate resolution is achievable by this standard. Direct detection sensitivities are usually quoted in terms of noise-equivalent power (NEP), while heterodyne sensitivities are usually given in terms of noise temperature, T_N. Conversion between the two systems is made via

$$\mathrm{NEP} = 2kT_N\sqrt{\Delta\nu}\,, \qquad (1)$$

where k is Boltzmann's constant (Storey 1985; Phillips 1988). With a bolometer NEP of 10^{-14} W $\mathrm{Hz}^{-1/2}$ and $\Delta\nu = 200$ MHz, the equivalent heterodyne receiver noise temperature would be 26,000 K, roughly 2 orders of magnitude higher than current SIS receiver capabilities (Phillips 1994), but only a factor of 4 or so above single sideband noise temperatures of Schottky diode receivers in use at the higher end of our frequency range (Harris et al. 1987; Howe et al. 1993). Of course this is not a completely fair comparison because of the 2–3 orders of magnitude greater bandwidth available with an FTS. Submillimeter FTS observations are thus ideally suited to observations of wide, bright lines, and to continuum observations, where the goal is very broadband information.

The FTS employed for those observations is an upgraded version of the interferometer used for holographic measurements of the Caltech Submillimeter Observatory (CSO) telescope surface (Serabyn, Masson, & Phillips 1991). It is a rapid-scan, dielectric-beam-splitter interferometer with a one-sided travel of 44 cm and a scan speed typically in the range 0.5–1.0 cm s^{-1} (Weisstein & Serabyn 1994). The resultant unapodized spectral resolution is 206 MHz, which corresponds to a velocity resolution ranging from 309 km s^{-1} at 200 GHz to 69 km s^{-1} at 900 GHz. For observations, the FTS is mounted at the CSO's Cassegrain focus. The interferometer operates in the open air, possible only because of the low-humidity conditions prevalent near the summit of Mauna Kea.

The broadband nature of an FTS implies that the observable range of frequencies is defined by the atmosphere transmission function. Figure 1*a* shows the millimeter/submillimeter zenith atmospheric transmission above Mauna Kea under relatively good observing conditions (1 mm precipitable H_2O). At submillimeter wavelengths, terrestrial H_2O and O_2 absorption lines limit observations to several transmission "windows" below 1 THz. To maximize sensitivity, astronomical spectra are measured with five metal-mesh filters available with the CSO facility bolometer, each matched to an atmospheric window (Fig. 1*b*). This combination provides access to frequencies ranging from just below 200 to near 900 GHz.

The instrumental field of view is defined by a Winston cone light concentrator (Harper et al. 1976) that illuminates the 0.3 K bolometric detector. For the observations presented below, we used a cone with an entrance aperture diameter equivalent to 31″ on the sky. Convolution of this cone's geometric response with the telescope's diffraction beam yields a beam FWHM (Fig. 2) that is 30″ ± 1″ over most of the range of interest.

For astronomical observations, pairs of interferometer scans (one in each direction of mirror motion) are successively made on and off source, as well as with an ambient-temperature blackbody source (Eccosorb) filling the beam. The scans are registered relative to each other by means of an absolute-position reference mark on the linear encoder that tracks the scanning mirror's position. Assuming the same physical temperature, T_{hot}, for the sky and the ambient (or "hot") load, this

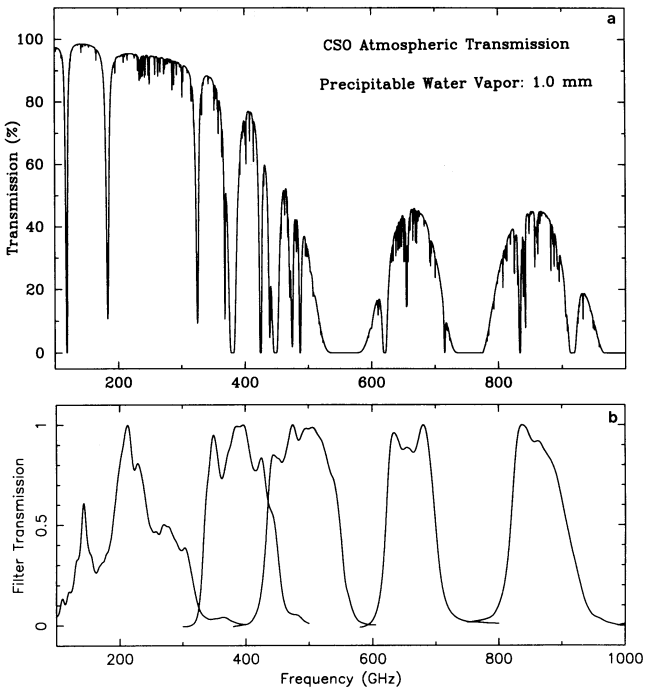

FIG. 1.—(*a*) Theoretical zenith atmospheric transmission above the CSO at millimeter and submillimeter wavelengths. (*b*) Transmission plots of the five broadband filters. From left to right, they are referred to in the text as the 1300, 800, 600, 450 and 350 μm filters.

set of scans allows a standard (on − off)/hot − off) correction for atmospheric attenuation and hot spillover (Penzias & Burrus 1973; Weisstein & Serabyn 1994). Because of the high frequencies involved, the measured voltage (V) ratio is scaled to the "Rayleigh-Jeans antenna temperature," T_A^*, using the full Planck expression for the hot-load flux:

$$T_A^* = \frac{h\nu/k}{(e^{h\nu/kT_{\mathrm{hot}}} - 1)}\,\frac{V_{\mathrm{on}} - V_{\mathrm{off}}}{V_{\mathrm{hot}} - V_{\mathrm{off}}}\,. \qquad (2)$$

Of course, the measured antenna temperatures are averages over spectral channels and so are lower than those obtained with spectral resolution sufficient to resolve lines. However, the integrated line areas, $\int T_A^*\,d\nu$, remain unaltered, and so it may be preferable to think of our observed T_A^* values (for unre-

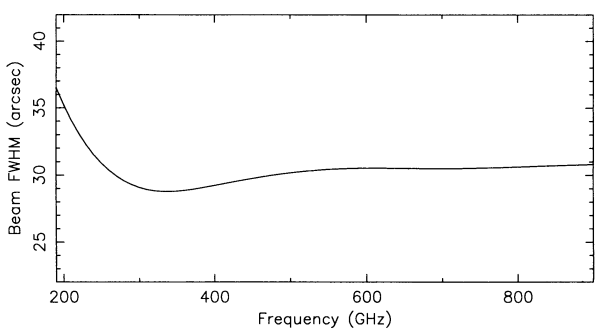

FIG. 2.—Calculated beam FWHM for the convolution of a 31″ circular aperture with an Airy pattern of FWHM = 27″ (230/ν), where ν is the frequency in GHz. The rise to low frequencies is due to increasing diffraction at long wavelengths.

solved lines) simply as line areas divided by the channel width, i.e.,

$$T_A^*(\text{obs}) = \frac{\int T_A^* dv}{\Delta v} . \quad (3)$$

Since T_A^*-defined line areas are the Rayleigh-Jeans analog of energy fluxes, the FTS can then be thought of as providing a direct measure of source line fluxes, making it very useful for studies of overall cloud energetics (albeit of broad-line sources only), as elaborated in § 6.

Under good weather conditions, the signal-to-noise ratio attained with the system has been confirmed to be consistent with theoretical performance expectations. For a single FTS scan, the expected signal-to-noise ratio is given by expression (9) of Serabyn et al. (1991). Allowing for the differencing of on- and off-source spectra and the accumulation of N on/off scan pairs, the root mean square (rms) noise in antenna temperature units becomes

$$\sigma = \frac{4\text{NEP}}{k} \sqrt{\frac{v}{c \Delta v N}} , \quad (4)$$

where v is the scan velocity and c is the speed of light. Since N is given by the total observing time, t, divided by twice the scan time, while the frequency resolution is inversely proportional to the scan length, this simplifies to

$$\sigma = \frac{4\text{NEP}}{k \Delta v \sqrt{2t}} , \quad (5)$$

With an NEP of 10^{-14} W Hz$^{-1/2}$, this becomes

$$\sigma \approx \frac{2}{\Delta v \sqrt{t}} , \quad (6)$$

where Δv is now in GHz and t is in seconds. In terms of line areas, the corresponding rms sensitivity is $\sigma \Delta v$. This performance was verified via an 0.9 hr long observation of M82 with the 800 μm filter (Fig. 3). While the measured rms noise level in Figure 3 is 0.17 K, evaluation of expression (4) with the relevant time yields 0.19 K. This observation also yielded a detection of the CO 3–2 line in this galaxy, with a line area (290 K MHz) consistent with previous heterodyne measurements (Tilanus et al. 1991).

The M82 spectrum illustrates both the possibilities and limitations of astronomical Fourier transform spectroscopy at submillimeter wavelengths. Given the lower sensitivity of direct detectors at these long wavelengths, Fourier transform spectroscopy obviously cannot compete with heterodyne instruments in single-line searches. Indeed, the CO detection in M82 is enabled only by the good match between the broad source line width and the instrumental resolution. On the other hand, the broadband nature of the measurements is unprecedented at these wavelengths, and it is this aspect which is exploited in the observations of the Orion molecular cloud which follow.

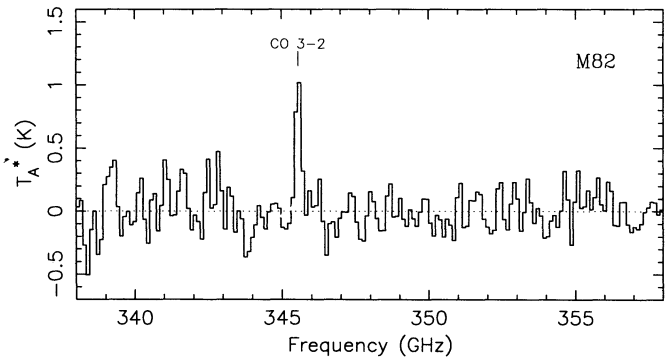

FIG. 3.—CO J = 3–2 line measured toward M82. The CO 3–2 tick mark is at a redshift of 200 km s^{-1}. The rms noise level is 0.17 K.

3. OBSERVATIONS AND DATA REDUCTION

Observations toward the position of IRc2 ($\alpha = 5^h32^m47^s$, $\delta = -5°24'24''$) in the core of the well-known Orion molecular cloud (OMC-1; Genzel & Stutzki 1989; Castets et al. 1990) were acquired with the 1300, 450, and 350 μm filters (Fig. 1*b*) on 1994 January 17, and with the 800 and 600 μm filters on 1994 March 19 and 20. For these initial observations, about an hour was spent observing with each filter, yielding a total observing time roughly equivalent to one Orion transit. The precipitable water vapor above the telescope varied substantially between the different observing dates, leading to differing noise levels in the five filter passbands, with particularly high noise in the 600 μm band (Fig. 4).

After Fourier-transforming the unapodized data, those sections of the spectra badly affected by terrestrial atmospheric lines were blanked out (in addition to broad H_2O and O_2 lines, narrow O_3 lines were problematic at a few frequencies), and then polynomial baselines (usually of first, but occasionally up to fourth order) were subtracted from the spectra in order to eliminate weather-related baseline curvature. Baseline subtraction deletes information on the continuum emission, but the weather was not stable enough to measure the continuum accurately in any case. This paper thus concerns itself exclusively with spectral line emission. The spectra were not apodized, so as not to degrade the spectral resolution, but were instead binned to channels of width approximately equal to the spectral resolution. The resultant spectra from each of the five filters were then combined into a single spectrum, shown in Figure 4 in both antenna temperature (T_A^*) and flux density units (the latter using the measured coupling of the spectrometer/telescope combination to Jupiter, $\approx$0.3 across all bands at the time of the observations). Between the bounds of 190 and 900 GHz, a total span of 360 GHz—51% of the range—has been measured, a coverage which vastly exceeds that provided by previous spectroscopic observations at these frequencies.

The spectrum in T_A^* units is also shown on an expanded horizontal scale in Figure 5. Two short sections of the spectrum have been omitted from Figure 5: 805–815 GHz (in which excessive noise due to the nearby atmospheric H_2O line allowed detection of only the strong CO 7–6 line) and 895–900 GHz (with no detections). In most of Figure 5, the rms noise level varies by roughly a factor of 2, between 0.18 and 0.36 K, but the fourth panel has substantially higher noise. To identify line detections in the spectrum, we applied a uniform cutoff of 2.5 σ, a level determined by a detailed comparison of our spectrum with the 215–263 GHz Owens Valley Radio Observatory (OVRO) (Sutton et al. 1985; Blake et al. 1986) and 325–360 GHz CSO (Groesbeck 1994; Schilke et al. 1995a) heterodyne surveys. Over most of the spectrum this cutoff corresponds to a detection limit of 85–170 K MHz. (However, near bright lines, the possibility of residual spectral ringing makes neighboring lines suspect even above the cutoff level.) Applying this 2.5 σ cutoff to the entire spectrum results in the identification of 187

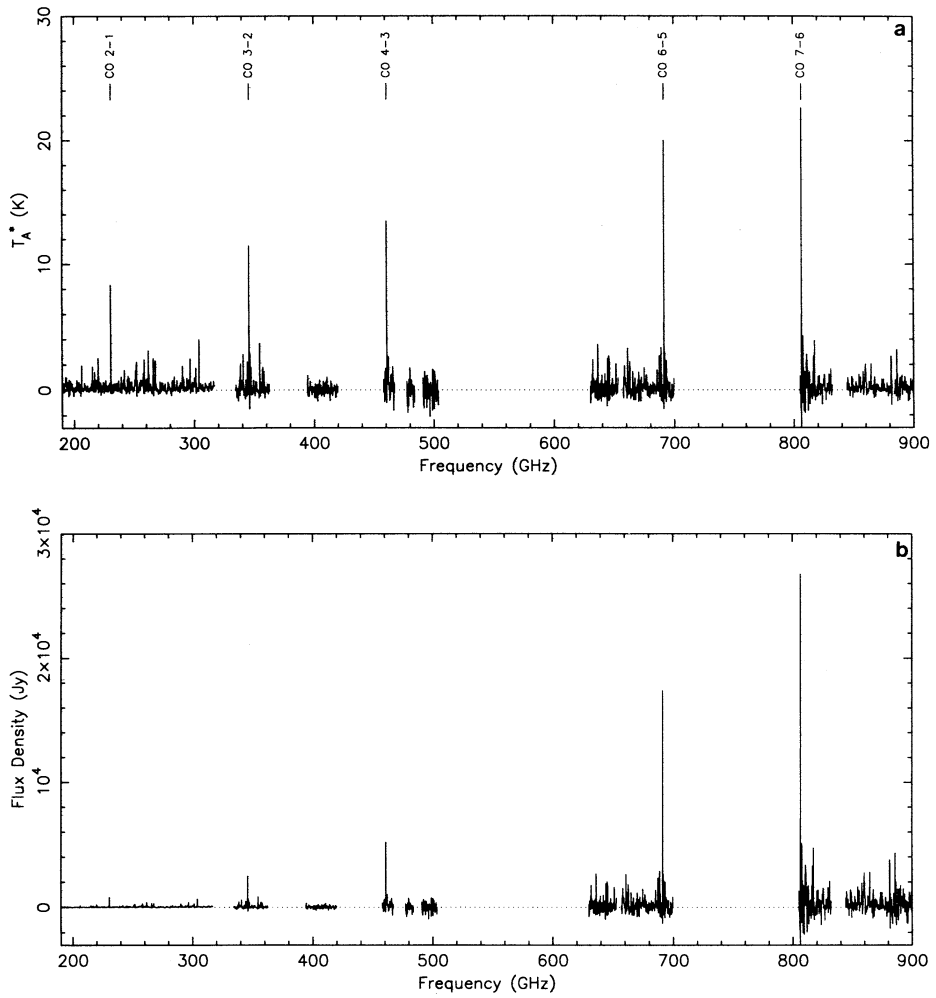

FIG. 4.—(*a*) Measured spectrum toward Orion IRc2 in Rayleigh-Jeans antenna temperature units, binned to frequency channels of 206 MHz (=resolution). (*b*) Measured spectral flux density for a source-coupling efficiency of 0.3.

spectral features (Fig. 5). One additional line ($H^{13}CN$ 8–7 at 690.6 GHz) is below the cutoff but is marked in Figure 5 because the baseline seems to dip anomalously to negative levels near that frequency, and the line is confirmed by heterodyne observations (Harris et al. 1995).

The spectral features marked in Figure 5 have been identified with the aid of the JPL line catalog (Pickett, Poynter, & Cohen 1992) and, in the ranges of overlap, by comparison to extant heterodyne surveys of the OMC-1 core (Sutton et al. 1984, 1995; Blake et al. 1985; Jewell et al. 1989; Greaves & White 1991; Groesbeck 1994; Schilke et al. 1995a; Harris et al. 1995; P. Schilke 1995, private communication). As a result, 182 of the detected features have been identified (Fig. 5) with transitions of 17 distinct molecular species (including isotopomers) in OMC-1. In most cases, several lines of a given species have been detected, easing identification. Of these 182 features 154 are attributed to specific transitions of individual molecules, 31 are identified as unresolved blends (or possible blends) of two lines, and two are likely triple blends. Roughly half of the transitions detected—the vast majority of those above 390 GHz, as well as most of those between 270 and 320 GHz—are first detections in the ISM. The highest frequency transition detected, at 893.6 GHz, is one of two transitions to the ground state of HDO (the other, at 464.9 GHz, was detected by Schulz et al. 1991).

Of the six remaining features in Figure 5, three could not be identified with lines from OMC-1 but are coincident with terrestrial O_3 frequencies and so are ascribed to O_3 contamination. Only three features then remain unidentified: 278.9, 659.0, and 869.5 GHz. The last of these is close to the frequencies of both the NaH 3–2 line and a highly excited H_2CO transition, but as all of these unidentified features barely exceed the detection cutoff, they could easily be due to noise. It is thus clear that no *strong* unidentified lines are present in the newly measured bands.

4. RESULTS

The most prominent lines evident in Figures 4 and 5 are the five CO lines which fall within our filter passbands. These are labeled in Figure 4 and originate in the $J = 2$, 3, 4, 6, and 7 upper rotational levels. The observed (unresolved) antenna temperatures of these CO lines increase nearly linearly with frequency (Fig. 4*a*), and their integrated line areas even more so (Fig. 6), with the best fit to the line areas given by $\int T_A^*(J \rightarrow J-1)\, dv = 0.96J + 0.05$ K GHz. This linear relationship is consistent with lines of roughly constant *bright-*

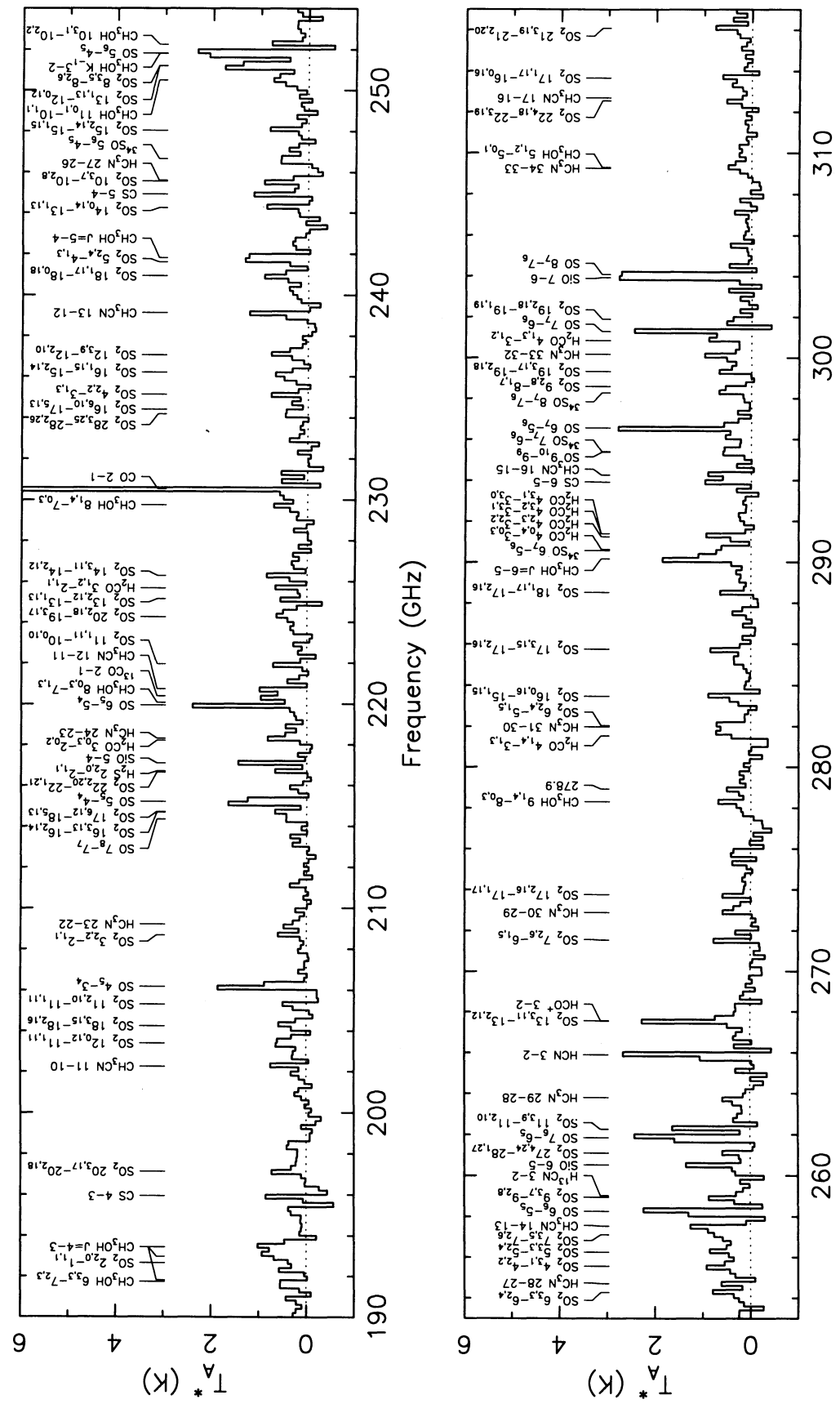

FIG. 5.—Orion spectrum binned to 200 MHz channels, with lines identified by molecule and quantum number (as in Gordy & Cook 1984 and Pickett et al. 1992). The 2.5 σ cutoff levels for line identification are 0.45 K for the first two panels, 0.55 K (0.7 K) for the left (right) section of the third panel, 1.3 K for the two leftmost sections of the fourth panel and 2.0 K for the third section, 0.9 K for the fifth panel, and 0.85 K below the break near 840 GHz and 0.65 K above for the last panel. Three possible unidentified lines are labelled by their frequencies, and three lines due to contamination by terrestrial O_3 are also identified.

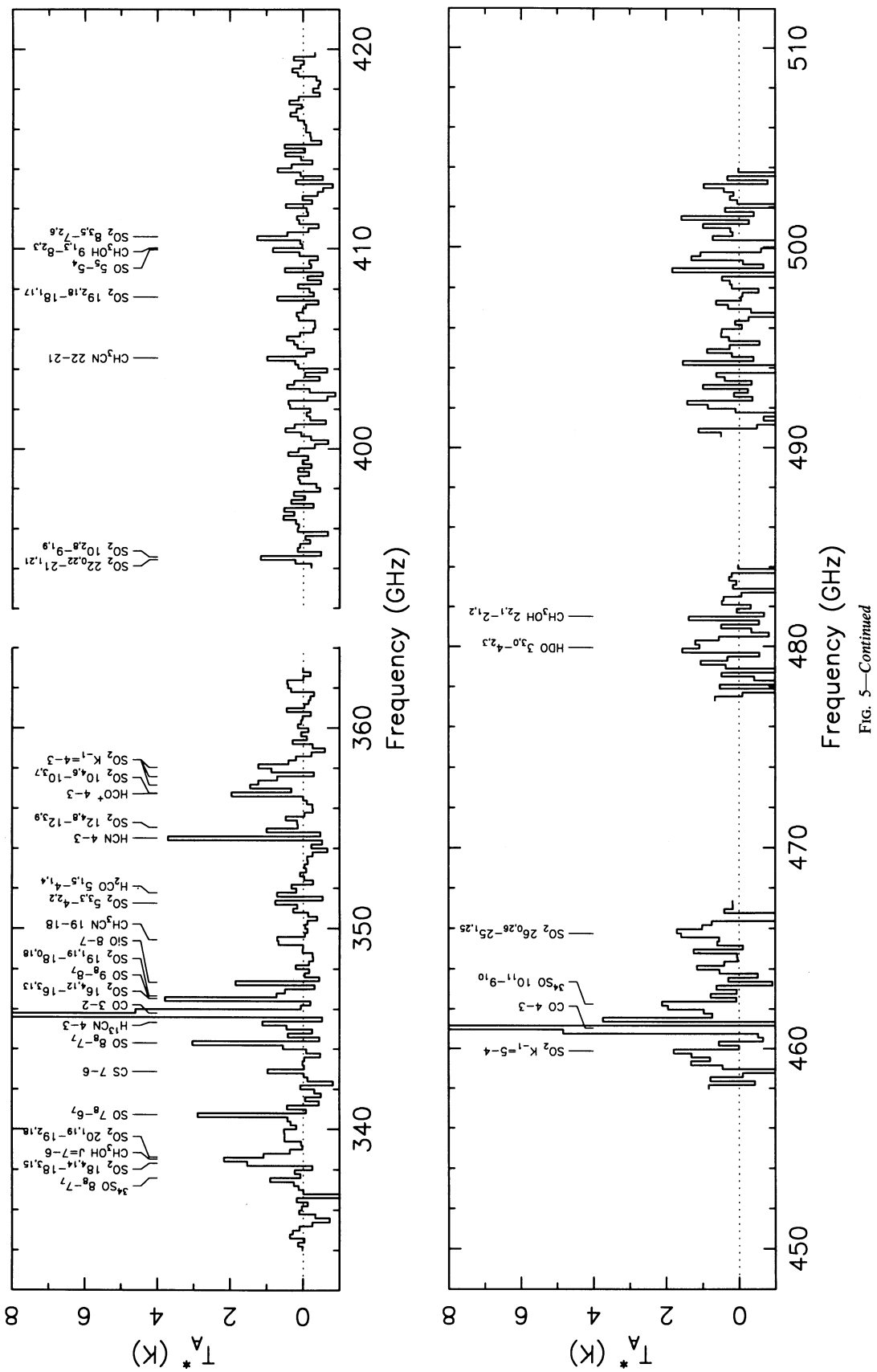

FIG. 5—*Continued*

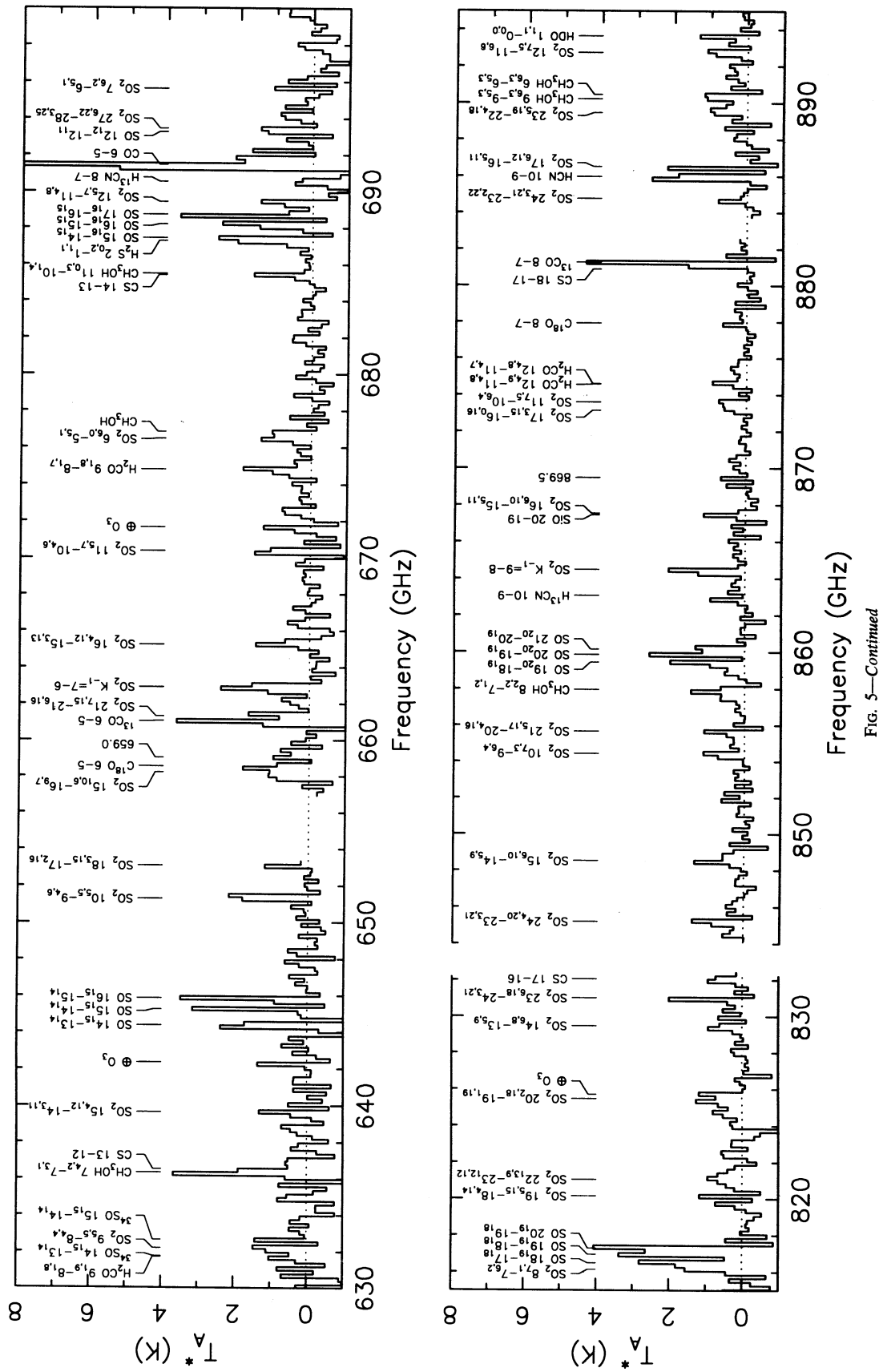

FIG. 5—*Continued*

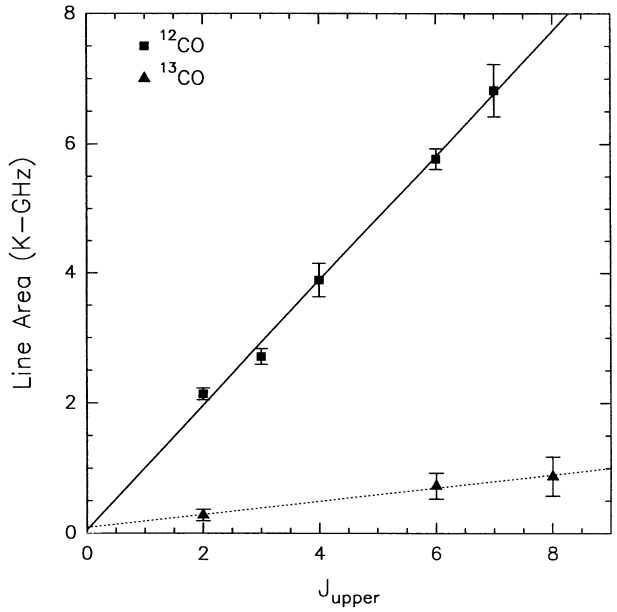

FIG. 6.—Integrated line areas ($\int T_A^* dv$) for ^{12}CO and ^{13}CO vs. the upper-level rotational quantum number. The error bars reflect the 2.5 σ detection threshold in most cases, except for the two highest ^{13}CO lines, where they also allow for the possibility of line blending. *Solid line*, $0.96J + 0.05$; *dashed line*, $0.10J + 0.09$.

ness temperature, owing both to the proportionality between Doppler line width and frequency (which causes line areas to increase in proportion to the frequency) and to the unresolved nature of our spectrum (in which antenna temperatures are line areas per channel). Thus, in the FTS spectrum, intrinsic brightness temperatures have a frequency dependence one power of ν lower than observed antenna temperatures. A series of constant brightness temperature lines then leads to antenna temperatures increasing linearly with ν, as is observed for CO, while conversely, a flat distribution of observed antenna temperatures implies a falloff of brightness temperatures with frequency.

Other than ^{12}CO, a similar rise in T_A^* with frequency is seen clearly only in ^{13}CO (Fig. 6). The ^{12}CO/^{13}CO line area ratios seem to be roughly independent of J, being 7.6, 7.9, and 8.8 (with 30% error bars) for the 2–1, 6–5, and 8–7 transitions, respectively (the latter requires extrapolating along the best-fit ^{12}CO line). The 2–1 ratio is consistent with previous heterodyne measurements in a similar beam size (Sutton et al. 1985). As the ^{12}C/^{13}C abundance ratio in OMC-1 is roughly 70 (Langer & Penzias 1990), large and surprisingly similar beam-averaged opacities are indicated for all of the ^{12}CO lines detected. While large opacities are directly implied by the J independence of the CO brightness temperatures, also required are roughly equal (and warm, $\gtrsim$100 K) kinetic temperatures in each line's formation region. This suggests that the detected CO lines, including even the low-J lines, emerge not from bulk or quiescent cloud material, but from warmer, UV- or shock-heated layers (e.g., Genzel & Stutzki 1989; Castets et al. 1990; Howe et al. 1993).

Excluding the well-studied CO molecule from consideration now, the brightest *non*-CO lines in the spectrum all show very similar antenna temperatures, roughly 3–4 K, independent of both frequency and molecule, consistent with decreasing excitation and/or opacity in the more highly excited lines. In addition, the non-CO spectrum has a decidedly "bunched" appearance, with several bright lines in ranges such as 250–268 GHz, 338–358 GHz, and 685–695 GHz. In contrast, other regions (e.g., 394–420 GHz) are completely devoid of bright lines (and so may be good regions in which to examine the continuum level). The primary reason for this bunching is that the majority of the brightest non-CO lines in the spectrum are from the SO molecule, which has strong rotational triplets (due to its $^3\Sigma$ ground electronic state; Gordy & Cook 1984) every 43 GHz. Since HCN, HCO^+, CH_3OH, SO_2, SiO, and, at high frequencies, ^{13}CO, also contribute emission lines with T_A^* similar to that of SO, the appearance of bunching occurs when a few lines from these molecules fall near an SO triplet.

While the strongest lines in Figures 4 and 5 are from the CO molecule, the most numerous (92, several of which are themselves bands) are from SO_2. The detected diatomic molecules include CO, ^{13}CO , C^{18}O, SO, ^{34}SO, CS, and SiO. Note that all of these diatomics involve only relatively abundant elements from groups IV and VI of the periodic table. Linear triatomics detected include HCN, H^{13}CN, and HCO^+. The only larger linear molecule seen is HC_3N while CH_3CN is the only symmetric top observed. Most of these larger molecules are based on the CN radical. Finally, the asymmetric tops detected include H_2CO, CH_3OH, SO_2, HDO, and H_2S (the latter via two blended lines only), all of which are simple combinations of IV/VI elements with each other, hydrogen, or both. These molecules (as well as H_2O—Cernicharo et al. 1994—which was not detected due to obscuration by telluric H_2O) are thus the dominant coolants of the OMC-1 core at $\nu \lesssim 1$ THz.

Although all of the molecules listed have been detected previously in OMC-1 via their lower frequency transitions, the much larger frequency coverage obtained here allows access to a host of additional transitions, thus providing an immediate overview of the cloud energetics, and also a quick-look characterization of the cloud chemistry. This wide-band information makes it clear that the heavier linear and symmetric top molecules (HC_3N and CH_3CN) emit primarily at the lower frequencies ($\nu \lesssim 500$ GHz), while the lighter diatomics, triatomics, and asymmetric tops emit throughout the observed range, consistent with simple partition function arguments. Differences are also seen among the light diatomic and triatomic linear rotors, with CO antenna temperatures rising toward high ν (remember that this implies constant brightness temperatures), the "density tracers" CS and HCN showing flattish distributions, SO being mainly flat, but with a slight decrease at the highest frequencies, and HCO^+ strong at low J, but undetected at high J (e.g., the 10–9 line).

In detail, lines of SO are seen to $N = 20$–19, HCN and H^{13}CN to $J = 10$–9, and CS to $J = 17$–16 (and likely to 18–17, but this line is blended with ^{13}CO 8–7). These highly excited lines arise in energy levels which lie above the ground state by as much as 234 K for HCN, 402 K for CS, and 447 K for SO and so require the presence of substantial temperatures ($\approx$90 K for SO; § 5) and densities. Since the "critical density" for excitation of a specific transition is equal to the ratio of the spontaneous emission rate, A, to the collisional de-excitation rate and A is given for linear rotors in the high-J limit by $A = 5.8 \times 10^{-12} \mu^2 \nu^3$ s^{-1} (where μ is the molecular dipole moment in debyes and ν is in GHz; Rohlfs & Wilson 1995), the similar dipole moments for SO (1.55 D), CS (1.96 D), and HCN (2.98 D) imply that the density regimes probed by transitions of these molecules are influenced very strongly by the choice of

observing frequency but only marginally by the choice of molecule. Thus, the SO, CS, and HCN transitions detected at $\nu > 800$ GHz all imply densities of $\sim 10^9$ cm^{-3} (e.g., Walmsley & Güsten 1994) if radiative trapping and infrared pumping can be ignored. However, as the observed (HCN 10–9)/($H^{13}CN$ 10–9) line rato is roughly 5, as compared to $^{12}C/^{13}C \sim 70$ (Langer & Penzias 1990), radiative trapping, and perhaps also infrared pumping, can lower the excitation requirements to $\sim 10^7$ cm^{-3} (Carroll & Goldsmith 1981; Ziurys & Turner 1986; Stutzki et al. 1988; Hauschildt et al. 1993). In either case, the high densities implied suggest that the emission in these high dipole moment linear rotors arises in shock-compressed gas, likely in the layer known as the plateau or doughnut (Plambeck et al. 1982) which surrounds the central outflow source. In contrast, the highest accessible transition of HCO^+ ($J = 10$–9 at 891.6 GHz) was not detected, implying that the high-frequency HCO^+ emission is at least a factor of 4 weaker than that of the very similar HCN molecule (cf. Stutzki et al. 1988 and Jaffe et al. 1992 for the $J = 9$–8 lines), likely reflecting the ion's tendency to be found in lower density regions (Vogel et al. 1984).

The detected molecules fall into several well-defined chemical families. First, all of the molecules other than SiO are composed exclusively of the five abundant elements H, C, N, O, and S (and their isotopes). Next, as mentioned above, the CN radical is prominent in four of the molecules. In addition, a sequence of increasingly hydrogenated compounds of CO is also present—CO, HCO^+, H_2CO, and CH_3OH are all seen (Millar 1993). However, absent from the list is any molecule containing the more weakly bound NO radical (Turner & Ziurys 1988), the third possible pairing of unlike CNO elements. Also absent, of course, are the symmetric pairings C_2, N_2, and O_2, the first two because of their lack of dipole transitions and the last because its magnetic dipole transitions are obscured by atmospheric O_2 emission. The SO bond is also well represented, by SO, ^{34}SO, and SO_2. Thus, molecules based on the CO, CN, and SO bonds (and their isotopic variants) account for 13 of the 17 molecules seen. Two further molecules, CS and SiO, are isoelectronic with CO, with corresponding elements from the third row of the periodic table in place of C or O. Finally, hydrogen bonding of the group VI elements O and S accounts for the saturated molecules H_2S and HDO, as well as the undetected H_2O molecule. Other simple saturated molecules, e.g., NH_3 and CH_4, are also present in OMC-1 (Pauls et al. 1983; Keene, Blake, & Phillips 1983; Lacy et al. 1991), but the former's fundamental rotational frequency of 572.5 GHz is blocked by the atmosphere, while the latter lacks a rotational dipole moment. Allowing for the FTS's sensitivity only to wide, bright lines, which effectively selects in favor of significant cooling lines, the wide FTS frequency coverage thus provides a quick census of the dominant broad-line radiators. Excluded from the spectrum are both symmetric molecules (with no rotational lines), and molecules with transition frequencies blocked by our atmosphere (both of which would remain inaccessible to any ground-based submillimeter spectrometer), and species with weak or narrow lines.

Regarding the last point, the emission from the OMC-1 core arises from several distinct cloud components, referred to as the "ridge," "hot core," and "plateau" features (Blake et al. 1987; Genzel & Stutzki 1989; Sutton et al. 1995), each with a distinct location, size, chemistry, and kinematic signature. Comparison with the low-frequency OVRO and CSO heterodyne surveys established that our moderate-resolution FTS measurements are sensitive primarily to the broad lines from the outflowing plateau gas ($\Delta v \sim 25$ km s^{-1}), although some narrower hot-core lines (e.g., HDO) are also seen. In particular, many of the molecules evident in the FTS spectrum, i.e., SO, SO_2, CS, H_2S, and SiO, have enhanced abundances in the plateau gas, presumably due either to gas-phase chemistry in shock-heated gas or to the liberation, via shocks, or refractory elements from dust grains (Blake et al. 1987; Millar 1993; Pineau des Forets et al. 1993). Since the lines detected by the FTS necessarily dominate the energy output from the OMC-1 core in our filter bands, it is evident that, in agreement with predictions based on lower frequency observations (Sutton et al. 1984), the outflowing plateau gas dominates the spectral line flux from the cloud core. This is true because of the plateau's combination of high temperature (a trait shared with the hot-core component) and broad line width (an outflow-specific trait), the latter allowing for lower opacities and the emergence of radiation across a broader bandwidth.

5. TEMPERATURES AND COLUMN DENSITIES

High gas temperatures in the OMC-1 core are directly indicated by emission arising in energy levels several hundred kelvins above the ground state. These temperatures, as well as molecular column densities, can be quantified using the "rotation diagram" technique (Schloerb et al. 1983; Blake et al. 1987). In this method, the population per sublevel is plotted against the energy of the upper level involved in the transition, the slope (on a semilog plot) then giving the temperature, and the y-intercept the column density. This technique is straightforward to apply to the FTS data because of its uniform calibration versus frequency. Here we apply it to the SO and SO_2 molecules because of the large number of strong transitions each shows in the spectrum. The rotation diagrams of SO, SO_2 and ^{34}SO are plotted in Figure 7 (including only the data for unblended lines and correcting for a beam efficiency of 0.3).

All of the SO_2 lines detected originate in levels less than 320 K above the ground state, and the data is well fitted by a single rotation temperature of 93 ± 5 K. Under the optically thin assumption (given the many similar-strength transitions of SO_2, individual opacities are likely not overly large), the implied beam-averaged column density is 8×10^{16} cm^{-2}. (Correction for high opacities would move a few of the lowest points upward and so decrease the scatter, but this is not a large effect.) Both of these values are in good agreement with earlier estimates made with similar-sized beams (Schloerb et al. 1983; Blake et al. 1987; Stutzki et al. 1989), but we note that the Blake et al. column density must first be scaled upward to account for main-beam coupling.

While the SO_2 data are well fitted by a single temperature, the SO data set (Fig. 7*b*) seems to suggest that two temperatures are called for: 36 ± 6 K at low J and 147 ± 17 K at high J. However, the more optically thin ^{34}SO transitions suggest otherwise (Fig. 7*c*), as they appear to be consistent with a single temperature of 100 ± 24 K. Furthermore, the high ^{34}SO antenna temperatures (compared to SO) imply that the SO emission is affected by opacity. Because of smaller line strengths at low J and falling populations at high J, a high SO column density would yield maximum opacities in midrange (i.e., at energy levels comparable to the rotation temperature), thereby effectively suppressing the mid-J lines. The observed effect of high opacity on the rotation diagram of a single-

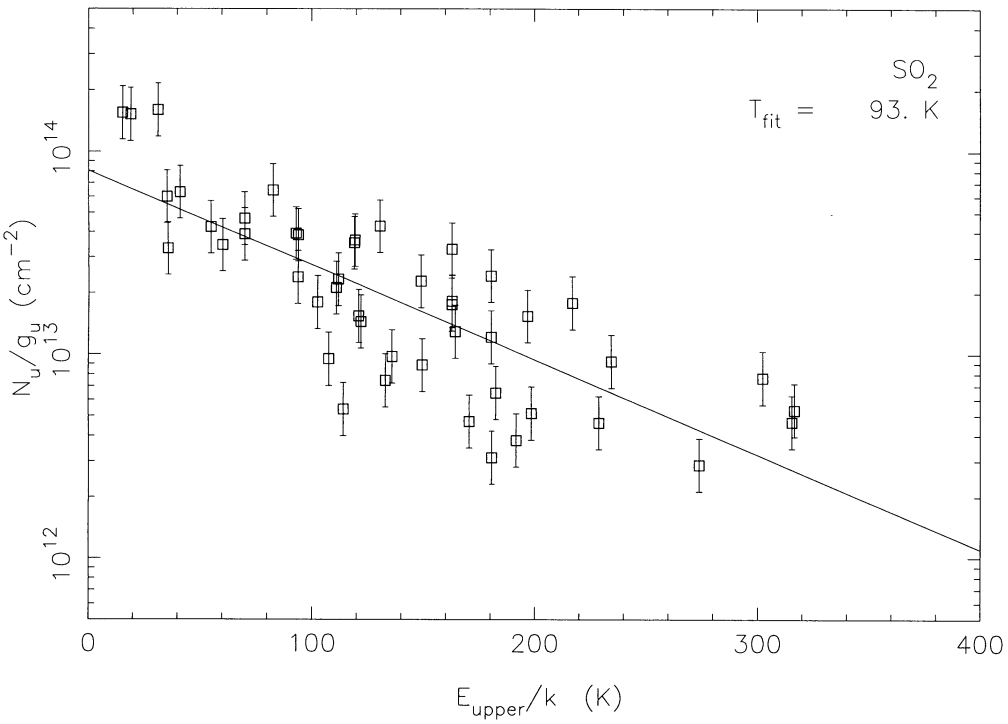

FIG. 7*a*

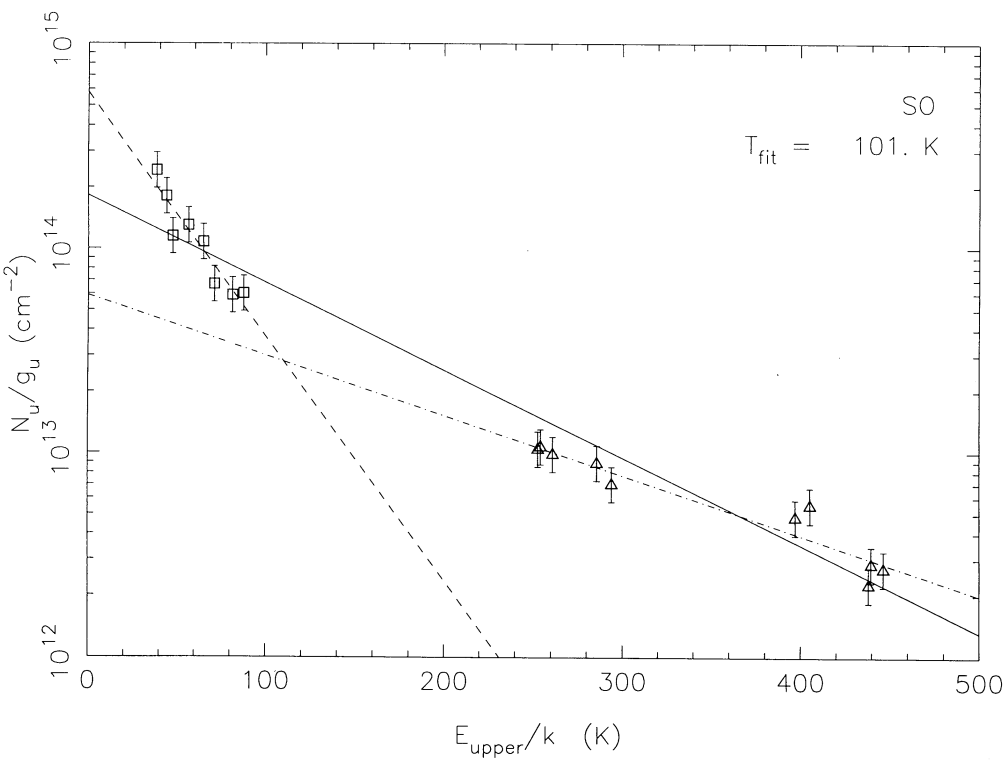

FIG. 7*b*

FIG. 7.—Excitation diagrams for (*a*) SO_2, (*b*) SO, and (*c*) ^{34}SO. N_u/g_u is the column density per sublevel in the upper level of each of the detected transitions, and E_{upper}/k is the upper-state energy level in kelvins. Single-temperature fits are plotted as solid lines, and the derived rotation temperatures are given in the upper right-hand corners. For SO, an optically thin single-component fit is not adequate, and so low-*J* (36 K, *boxes*) and high-*J* (147 K, *triangles*) fits are also included as dashed and dash-dotted curves, respectively. (*d*) SO level populations corrected for opacity effects (as described in the text), and a single-component fit is again given.

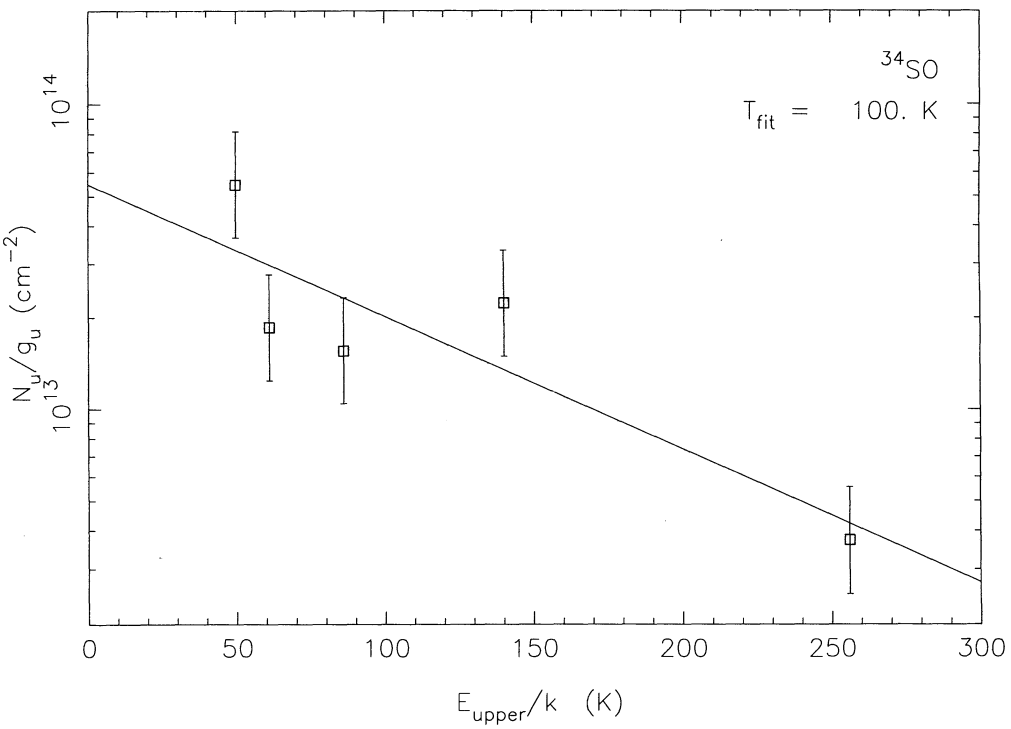

FIG. 7*c*

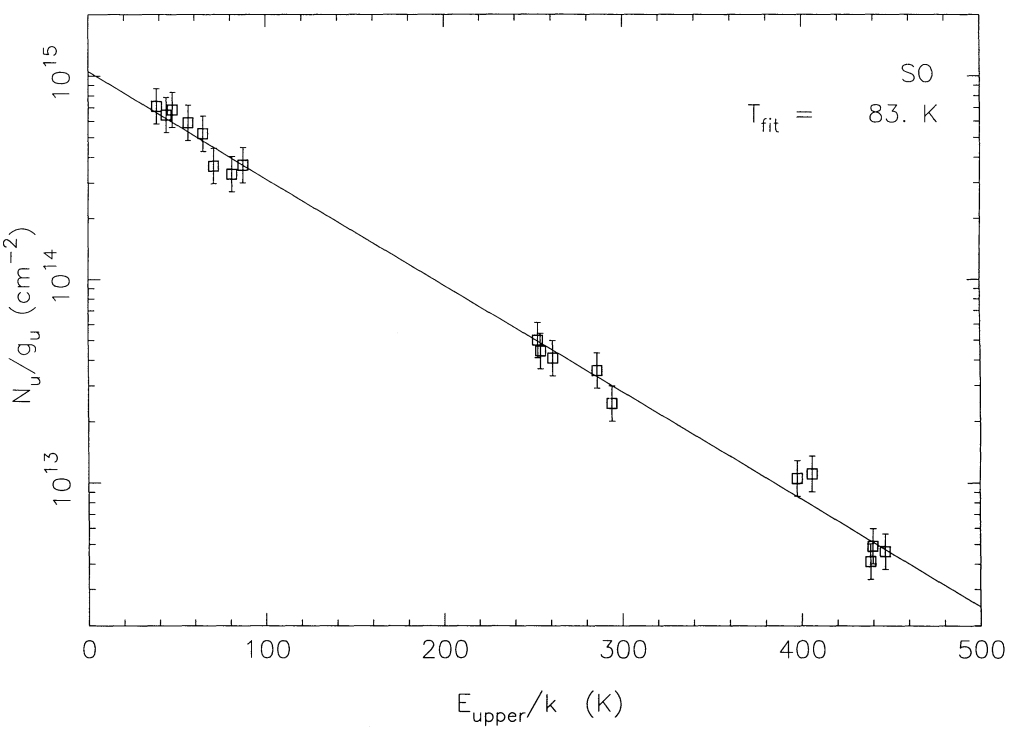

FIG. 7*d*

TABLE 1

TEMPERATURES AND COLUMN DENSITIES OF S-BEARING MOLECULES IN THE PLATEAU

Species	T_{rot} (K)	Column Density (molecules cm^{-2})	Abundance $N_{H_2} = 10^{23}$ cm^{-2}	Abundance $N_{H_2} = 10^{24}$ cm^{-2}
SO	83	2.2×10^{17}	2.2×10^{-6}	2.2×10^{-7}
^{34}SO	100	1.4×10^{16}	1.4×10^{-7}	1.4×10^{-8}
SO_2	93	8.0×10^{16}	8.0×10^{-7}	8.0×10^{-8}

temperature source would then be to push the midrange points downward, thus mimicking a dual-temperature source.

To see whether this is the case for SO, we attempted to correct for opacity in the SO transitions by using the additional information supplied by the ^{34}SO lines (Fig. 7*c*). With a rotation temperature of 100 K and a column density of 1.4×10^{16} cm^{-2} for ^{34}SO, and assuming an abundance ratio for ^{32}S/^{34}S of 16 (Schloerb et al. 1983; Blake et al. 1987), the column density of SO becomes 2.2×10^{17} cm^{-2}. The opacities resulting from this column of SO were then calculated from their intrinsic line strengths using the SIMCAT software described by Groesbeck (1994). This step requires knowledge of the line width, for which we used values appropriate to the plateau component, 25 km s^{-1}. The resultant opacities, τ, ranged from roughly 3 for our lowest frequency transition, to 6 in midrange, to 1.2 for the highest frequency lines. The line fluxes were then scaled upward by $\tau/(1 - e^{-\tau})$, the inverse of the escape probability (Schloerb et al 1983), to yield the opacity-corrected rotation diagram shown in Figure 7*d*.

In contrast to the original diagram, Figure 7*d* is consistent with a single-temperature solution. The best-fit rotational temperature is 83 ± 2 K, which is slightly below but within the error bars for the starting ^{34}SO temperature. The resultant column density is identical to the starting value of 2.2×10^{17} cm^{-2}. The column density is consistent with estimates based on observations of a few low-frequency, low-opacity transitions (Plambeck et al. 1982; Friberg 1984) but is well above the estimate of Blake et al. 1987 (which is based on more opaque higher frequency lines but is uncorrected for either main-beam efficiency or opacity).

Several results emerge from this analysis. First, it is apparent that multiple gas temperatures can effectively be mimicked by opacity effects. Second, after correcting for optical depth effects in SO as outlined above, the temperatures of all three S-bearing plateau species come into good agreement. Averaging over the species, a representative value for SO, ^{34}SO, and SO_2 in the plateau is then 90 K. Third, in the plateau, the [SO/SO_2] column density ratio is ≈ 3. Finally, assuming a canonical H_2 column density of 10^{23} cm^{-2} (Blake et al. 1987), abundances relative to H_2 of 2.2×10^{-6} for SO and 8×10^{-7} for SO_2 are deduced for the plateau gas. As the abundance of H_2S in the plateau is 4×10^{-6} (assuming the same H_2 column density; Minh et al. 1990), the sum of the abundances of these three S-bearing molecules relative to H_2 is 7×10^{-6}. More than 20% of all S would then be in molecular form. Alternatively, the column density of H_2 in the plateau may well be much higher, as argued by Schilke, Phillips, & Wang (1995b). With an H_2 column density of 10^{24} cm^{-2}, only 2% of the sulfur would be tied up in these molecular forms, and a sulfur depletion of up to 50 would be possible. These results are summarized in Table 1.

6. ENERGETICS

In the observed bands, the total molecular line flux in our beam is 5.7×10^{-10} ergs s^{-1} cm^{-2}, of which the SO_2, CO, and SO molecules together radiate three-quarters (Table 2, cols. [2] and [3]). Of the other molecules seen, ^{13}CO and CH_3OH each contribute 4%–5% of the flux and the remaining species contribute no more than about 2% each. The contributions of molecules—e.g., HCN, and especially H_2O—with spectra not well sampled by the available atmospheric transmission windows are necessarily underestimated. Of course, emission from weaker transitions not detected by the FTS is also excluded.

Although the fluxes given in Table 2 depend on both the beam size and beam-coupling correction, as well as on the bandpass of the available atmospheric transmission windows, the flux *ratios* are representative of the source. In particular, the preeminent role of SO_2 is consistent with lower frequency observations (Sutton et al. 1984; Groesbeck 1994). Furthermore, as the average line fluxes in the ranges 215–247 and 247–263 GHz (28 and 45 Jy, respectively), are quite similar to the OVRO heterodyne results for these ranges (Sutton et al. 1984), our calibration is corroborated.

To more accurately estimate the energies radiated by the three dominant molecules, and indeed by all molecules, below our upper frequency limit of 900 GHz, the measured fluxes must be corrected for unobserved lines between the measured bands. For CO this correction is simple, given the quite linear dependence on J of its integrated line areas (in K GHz). Because of the approximate validity of the Rayleigh-Jeans approximation, the CO line flux then increases roughly as the cube of the frequency, with $\sim 2.3 \times 10^{-13} J^3$ ergs s^{-1} cm^{-2} in each successive line. The missing $J = 1$–0 and $J = 5$–4 fluxes are therefore easily interpolated, yielding 0.29×10^{-10} ergs s^{-1} cm^{-2} in these two lines. The total flux radiated by CO below 900 GHz is then only 20% higher than observed. For SO, the correction is nearly as straightforward since the large number of observed triplets also allows for a ready interpolation (ignoring the few weaker non-triplet lines seen). The high noise near the 19–18 triplet (at 817 GHz) introduces some

TABLE 2

MOLECULAR LINE FLUXES

Species (1)	Observed Line Flux (10^{-10} ergs s^{-1} cm^{-2}) (2)	Observed Line Flux Fraction (3)	Predicted 0–900 GHz Line Flux (10^{-10} ergs s^{-1} cm^{-2}) (4)	Predicted 0–900 GHz Flux Fraction (5)
SO_2	1.7	29%	4.0	35%
SO	1.1	19	2.3	20
CO	1.5	27	1.8	16
SO_2 + SO + CO	4.3	75	8.1	72
All molecules	5.7	100	11.3	100

uncertainty, and so several fits were made to the flux density versus frequency data: linear and cubic fits were made to all eight observed SO triplets, as well as to the subset of seven triplets excluding 19–18. All four fits yielded $\approx 2.3 \times 10^{-10}$ ergs s^{-1} cm^{-2} for the flux in SO lines below 900 GHz. Thus for SO, the large number of missing lines (a triplet every 43 GHz) implies an upward correction to the flux of slightly more than a factor of 2. For SO_2, with its many asymmetric top transitions, it is possible to begin from the assumption that the SO_2 lines are more or less uniformly distributed across all frequencies, so that at low enough resolution the emergent flux is a smooth function of frequency. Averaging the observed SO_2 lines over $\sim$30-GHz-wide intervals, this smoothed SO_2 flux was fit with both linear and cubic polynomials, both of which gave fluxes of about 4.0×10^{-10} ergs s^{-1} cm^{-2} for SO_2 below $\nu = 900$ GHz. The corrected fluxes are summarized in column (4) of Table 2.

After correction for missing lines, both the SO and SO_2 molecules are found to emit more strongly than CO in the 0–900 GHz frequency range by factors of roughly 1.3 and 2.2, respectively. The upward revisions to the SO and SO_2 contributions are not very dependent on the specific extrapolations and arise simply because most of the CO lines below 900 GHz happen to lie in clear atmospheric windows, so that most of the CO molecule's energy output can be seen directly, while molecules with more closely spaced lines must necessarily radiate a proportional amount of their energy into the unobserved bands (in our measurements, 49% of the interval between 190 and 900 GHz). The exact ratios given above do depend on the cutoff frequency used in the comparison (especially if placed near a CO line), and our upper frequency cutoff of 900 GHz is certainly arbitrary. However, even in round numbers, SO_2 is clearly the most prolific radiator in the OMC-1 core below 1 THz—by about a factor of 2. While SO also exceeds CO in output in the 0–900 GHz range, CO's smaller mass implies that its radiative output can extend to higher frequencies, and so CO's total output may well exceed that of SO. Crude extrapolations of our data suggest that this crossover may occur near 1 THz.

Finally, we turn to the total line emission. To this end, Figure 8 presents the measured spectral flux density binned to a resolution of 9 GHz. This lower resolution version of the spectrum can be described by two components—a series of spikes at the CO frequencies and a relatively smooth "quasi-continuum" component, F_ν, which generally increases with frequency (but which also has significant regions with little flux near 400 and 500 GHz). As the smooth component shows little or no evidence of leveling off at the highest frequencies observed, it is possible to fit this component adequately with a simple quadratic function. Fitting all of the data except for the CO points yields $F_\nu = 3.6 \times 10^{-4} \nu_{\rm GHz}^2$ Jy, while excluding also the almost flux-free regions near 400 and 500 GHz allows a better fit to the high-frequency points and increases the coefficient only slightly to 3.9×10^{-4}. The latter curve is plotted in Figure 8. This quadratic frequency dependence results predominantly from the conversion to flux densities of the antenna temperatures of the brighter non-CO lines detected, which, as was pointed out earlier, are roughly constant at 3–4 K. This provides some reason to believe that the fitted curve is also capable of describing the flux density in the gaps between the measured bands. However, the H_2O molecule remains an unknown, as does the net contribution of the numerous weaker lines which are below the detection limit.

The integrated flux arising from the observed non-CO lines then increases roughly as $\int_0^\nu F_\nu \, d\nu \approx 1.3 \times 10^{-18} \nu_{\rm GHz}^3$ ergs s^{-1} cm^{-2}, for a total of 9.5×10^{-10} ergs s^{-1} cm^{-2} below 900 GHz. With 1.8×10^{-10} ergs s^{-1} cm^{-2} in CO lines, the total line flux below 900 GHz is 11.3×10^{-10} ergs s^{-1} cm^{-2}. Knowledge of this total allows the true percentages radiated by CO, SO, and SO_2 below 900 GHz to be calculated (Table 2, col. [5]). As is evident from the table, below 900 GHz SO_2 radiates roughly one-third the total line flux, and together, the S-bearing molecules SO_2 and SO radiate over half the flux, making molecules based on the SO bond the dominant molecular emitters of spectral line energy in the OMC-1 core. Oxygenated sulfur molecules thus evidently serve as very effective radiators of the shock energy to which they owe their existence. Of course, from an atomic viewpoint, the single most important constituent of the radiating molecules is oxygen, as the four O-bearing molecules SO_2, SO, CO, and ^{13}CO together radiate 80% of the energy.

Finally, although the smooth quasi-continuum flux density due to the ensemble of observed non-CO lines increases as the square of the frequency, the CO line *fluxes* increase as the cube of the frequency. This implies that the CO lines become increasingly important at higher frequencies. In order of increasing J, the five observed CO lines have quasi-continuum equivalent widths of 10, 13, 18, 27, and 32 GHz, respectively.

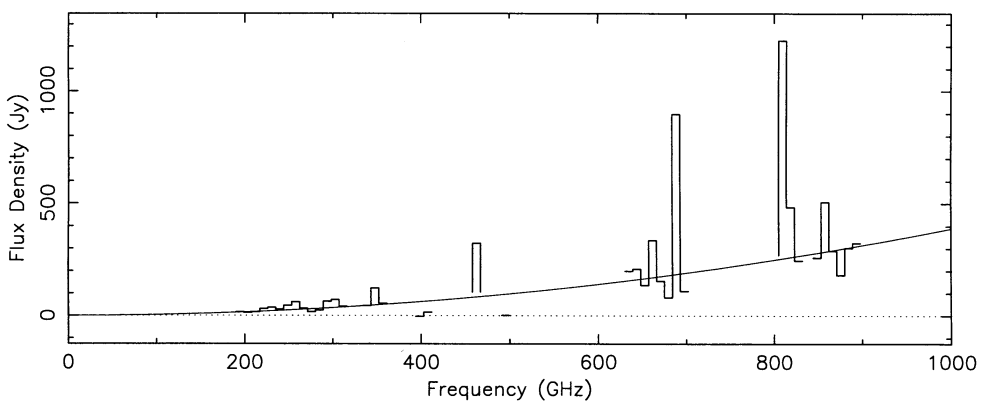

FIG. 8.—Measured spectral flux density of Fig. 4*b* binned to 9 GHz resolution. The points at 652.5 and 697.5 GHz are extrapolations for partially filled frequency bins. The solid curve, given by $F_\nu = 3.9 \times 10^{-4} \nu_{\rm GHz}^2$ Jy, is the fit to the flux density for all non-CO lines above our detection threshold, excluding the region between 400 and 500 GHz.

Considering all detected line emission in frequency intervals equal to the CO line spacing (115 GHz), the CO lines then contribute roughly 8%, 10%, 14%, 19%, and 22%, respectively, of the measured line fluxes in these bands. Weaker lines below the detection threshold imply that these percentages are more accurately upper limits to the contributions of the CO fluxes.

7. FUTURE PROSPECTS

The techniques presented here represent a significant addition to the submillimeter observational repertoire. Given the necessarily quick-look nature of these initial observations, longer integration times and better weather offer the prospect of further signal-to-noise improvements, which should allow for improved measurements of Orion, and also of more distant sources. Technical issues also allow for further progress since, in the more unexplored high-frequency bands, smaller beamwidths should yield increased source couplings and antenna temperatures on compact sources, and broader filters should allow access to even wider spectral bands. In addition, as our velocity resolution at $\nu = 900$ GHz is only about 3 times the width of the OMC-1 plateau feature, a modest increase in spectral resolution would be quite productive. Finally, the determination of the shape of submillimeter continuum emission (not obtained in this initial study) and measurement of the line-to-continuum ratio remain important goals.

We are especially grateful to P. Schilke for many informative discussions, and for providing access to several data sets, both published and unpublished. We also thank G. A. Blake, P. G. Green, T. D. Groesbeck, A. I. Harris, and T. G. Phillips for providing data prior to publication, and for helpful discussions. We thank the referee for well-directed comments. This work and the CSO are supported by NSF grant AST 93-13929.

REFERENCES

Blake, G. A., Sutton, E. C., Masson, C. R., & Phillips, T. G. 1986, ApJS, 60, 357
———. 1987, ApJ, 315, 621
Brault, J. W. 1985, in High Resolution in Astronomy: 15th Adv. Course Swiss Soc. Astrophys., ed. A. Benz, M. Huber, & M. Mayor (Sauverny: Geneva Observatory), 1
Carroll, T. J., & Goldsmith, P. F. 1981, ApJ, 245, 891
Castets, A., Duvert, G., Dutrey, A., Bally, J., Langer, W. D., & Wilson, R. W. 1990, A&A, 234, 469
Cernicharo, J. 1991, in The Physics of Star Formation and Early Stellar Evolution, ed. C. J. Lada & N. D. Kylafis (Dordrecht: Kluwer), 287
Cernicharo, J., Gonzales-Alfonso, E., Alcolea, J., Bachiller, R., & John, D. 1994, ApJ, 432, L59
Cummins, S. E., Linke, R. A., & Thaddeus, P. 1986, ApJS, 60, 819
Friberg, P. 1984, A&A, 132, 265
Genzel, R. 1991, in The Physics of Star Formation and Early Stellar Evolution, ed. C. J. Lada & N. D. Kylafis (Dordrecht: Kluwer), 155
Genzel, R., & Stutzki, J. 1989, ARA&A, 27, 41
Gordy, W., & Cook, R. L. 1984, Microwave Molecular Spectra (New York: Wiley)
Greaves J. S., & White, G. J. 1991, A&AS, 91, 237
Groesbeck, T. D. 1994, Ph.D. thesis, Caltech
Harper, D. A., Hildebrand, R. H., Stiening, R., & Winston, R. 1976, Appl. Opt., 15, 53
Harris, A. I., Avery, L. W., Schuster, K. F., Tacconi, L. J., & Genzel, R. 1995, ApJ, in press
Harris, A. I., Jaffe, D. T., Stutzki, J., & Genzel, R. 1987, Int. J. Infrared Millimeter Waves, 8, 857
Hauschildt, H., Güsten, R., Phillips, T. G., Schilke, P. Serabyn, E., & Walker, C. K. 1993, A&A, 273, L23
Howe, J. E., Jaffe, D. T., Grossman, E. N., Wall, W. F., Mangum, J. G., & Stacey, G. J. 1993, ApJ, 410, 179
Irvine, W. M., Goldsmith, P. F., & Hjalmarson, A. 1987, in Interstellar Processes, ed. D. J. Hollenbach & H. A. Thronson, Jr. (Dordrecht: Reidel), 561
Jaffe, D. T., Graf, U. U., Harris, A. I., Stutzki, J., & Lepp, S. H. 1992, ApJ, 385, 240
Jewell, P. R., Hollis, J. M., Lovas, F. J., & Snyder, L. E. 1989, ApJS, 70, 833
Johansson, L. E. B., et al. 1984, A&A, 130, 227
Keene, J. B., Blake, G. A., & Phillips, T. G. 1983, ApJ, 271, L27
Lacy, J. H., Carr, J. S., Evans, N. J., II, Baas, F., Achtermann, J. M., & Arens, J. F. 1991, ApJ, 376, 556
Langer, W. D., & Penzias, A. A. 1990, ApJ, 357, 477
Millar, T. J. 1993, in Dust and Chemistry in Astronomy, ed. T. J. Millar & D. A. Williams (Bristol: IOP), 264
Minh, Y. C., Ziurys, L. M., Irvine, W. M., & McGonagle, D. 1990, ApJ, 360, 136
Pauls, T. A., Wilson, T. L., Bieging, J. H., & Martin, R. N. 1983, A&A, 124, 23
Penzias, A. A., & Burrus, C. A. 1973, ARA&A, 11, 51
Phillips, T. G. 1988, in Millimetre and Submillimetre Astronomy, ed. R. D. Wolstencroft & W. B. Burton (Dordrecht: Kluwer), 1
Phillips, T. G. 1994, in IAU Colloq. 140, Astronomy with Millimeter and Submillimeter Wave Interferometry, ed. M. Ishiguro & W. J. Welch (San Francisco: ASP), 68
Phillips, T. G., & Keene, J. 1992, Proc. IEEE, 80, 1662
Pickett, H. M., Poynter, R. L., & Cohen, E. A. 1992, JPL Publ. 80-23, Rev. 3
Pineau des Forêts, G., Roueff, E., Schilke, P., & Flower, D. R. 1993, MNRAS, 262, 915
Plambeck, R. L., Wright, M. C. H., Welch, W. J., Bieging, J. H., Baud, B., Ho, P. T. P., & Vogel, S. N. 1982, ApJ, 259, 617
Rohlfs, K., & Wilson, T. L. 1995, Tools of Radio Astronomy (2d ed.; Berlin: Springer)
Schilke, P., Groesbeck, T. D., Blake, G. A., & Phillips, T. G. 1995a, in preparation
Schilke, P., Phillips, T. G., & Wang, N. 1995b, ApJ, 441, 334
Schloerb, F. P., Friberg, P., Hjalmarson, A., Höglund, B., & Irvine, W. M. 1983, ApJ, 264, 161
Schnopper, H. W., & Thompson, R. I. 1974, in Methods of Experimental Physics, vol. 12A, Astrophysics, ed. N. Carlton (New York: Academic), 491
Schulz, A., Güsten, R., Serabyn, E., & Walmsley, C. M. 1991, A&A, 246, L55
Serabyn, E., Phillips, T. G., & Masson, C. R. 1991, Appl. Opt., 30, 1227
Storey, J. W. V. 1985, Infrared Phys., 25, 583
Stutzki, J., Genzel, R., Graf, U. U., & Harris, A. I. 1989, ApJ, 340, L37
Stutzki, J., Genzel, R., Harris, A. I., Herman, J., & Jaffe, D. T. 1988, ApJ, 330, L125
Sutton, E. C., Blake, G. A., Masson, C. R., & Phillips, T. G. 1984, ApJ, 283, L41
———. 1985, ApJS, 58, 341
Sutton, E. C., Jaminet, P. A., Danchi, W. C., & Blake, G. A. 1991, ApJS, 77, 255
Sutton, E. C., Peng, R., Danchi, W. C., Jaminet, P. A., Sandell, G., & Russel, A. P. G. 1995, ApJS, 97, 455
Tilanus, R. P. J., Tacconi, L. J., Sutton, E. C., Zhou, S., Sanders, D. B., Wynn-Williams, C. G., Lo, K. Y., & Stephens, S. A. 1991, ApJ, 376, 500
Turner, B. E. 1989, ApJS, 70, 539
———. 1991, ApJS, 76, 617
Turner, B. E., & Ziurys, L. M. 1988, in Galactic and Extragalactic Radio Astronomy, ed. G. L. Vershuur & K. I. Kellerman (Berlin: Springer), 200
van Dishoeck, E. F., Blake, G. A., Draine, B. T., & Lunine, J. I. 1993, in Protostars and Planets III, ed. E. H. Levy & J. I. Lunine (Tucson: Univ. Arizona Press), 163
Vogel, S. N., Wright, M. C. H., Plambeck, R. L., & Welch, W. J. 1984, ApJ, 283, 655
Walmsley, C. M., & Güsten, R. 1994, in The Structure and Content of Molecular Clouds, ed. T. L. Wilson (Berlin: Springer), 164
Weisstein, E. W., & Serabyn, E. 1994, Icarus, 109, 367
Wright, E. L., et al. 1991, ApJ, 381, 200
Ziurys, L. M., & McGonagle, D. 1993, ApJS, 89, 155
Ziurys, L. M., & Turner, B. E. 1986, ApJ, 300, L19